1 **Late Diagenesis of Illite-Smectite in the Podhale Basin: Chemistry, Morphology and**

2 **Preferred Orientation**

3

4

5 Ruarri J. Day-Stirrat[1][*], Andrew C. Aplin[2], Kuncho D. Kurtev[3], Anja M. Schleicher[4], Andrew P.

6 Brown[5] and Jan Środoń[6]

7

8 [1] Shell International E&P Inc, Shell Technology Center-Houston, 3333 Highway 6 South,

9 Houston, Tx, 77082, USA

10 [2] Department of Earth Sciences, Durham University, Durham, DH1 3LE, U.K.

11 a.c.aplin@durham.ac.uk

12 [3] SINTEF, Sem Sælands vei 11, 7034, Trondheim, Norway. Kuncho.Kurtev@sintef.no

13 [4] Helmholtz Centre Potsdam,GFZ German Research Centre for Geosciences, Telegrafenberg,

14 Building B, room 327, 14473 Potsdam, Germany. anja.maria.schleicher@gfz-potsdam.de

15 [5] Institute for Materials Research, University of Leeds, Leeds, LS2 9JT, UK.

16 A.P.Brown@leeds.ac.uk

17 [6] Institute of Geological Sciences, PAN, Senacka 1, 31-002 Kraków, Poland ndsrodon@cyf-

18 kr.edu.pl

19 *Corresponding Author:

20 Dr. Ruarri J. Day-Stirrat

21 Shell International E&P Inc, Shell Technology Center-Houston, 3333 Highway 6 South, Houston,

22 Tx, 77082, USA

23 E-mail: ruarri.day-stirrat@shell.com

24

Abstract

25

26   Well-characterized samples from the Podhale Basin, southern Poland, formed the basis for

27   exploring and illuminating subtle diagenetic changes to a mudstone towards the upper end of the

28   diagenetic window, prior to metamorphism. Transmission Electron Microscopy (TEM)

29   performed on dispersed grains and ion-beam thinned preparations, Selected Area Diffraction

30   Patterns (SAED) and chemistry by TEM-EDS (Energy Dispersive Spectra) augmented

31   mineralogy and fabric data. The deepest samples show no change in their percent illite in illite-

32   smectite (I-S), yet I-S phase octahedral Fe^{3+} and Al^{3+} are statistically different between samples.

33   A decrease in the in the Fe^{3+} concentration in the octahedral sheet correlates with an increase in

34   I-S fabric intensity and apparent crystallinity. The D-statistic from the Kolmogorov-Smirnov (K-

35   S) test on TEM-EDS data describes statistical differences between the I-S chemistry. Previous

36   work on these samples showed a significant increase in the preferred orientation of the I-S phase

37   across the smectite-to-illite transition and a significant slowdown in the rate of development of

38   preferred orientation beyond the termination of smectite illitization. Lattice fringe images

39   describe an I-S morphology that coalesces into large and tighter packets with increasing burial

40   temperature and a decrease in I-S packet contact angle, yet some evidence for smectite collapse

41   structures is retained. The deepest sample shows the thickest, most coherent I-S packets. We

42   propose that the deepest samples in the Podhale Basin describe the precursor stage in

43   phyllosilicate fabric preferred orientation increase from diagenesis into metamorphism, where

44   continued evolution of crystallite packets and associated crystallinity create higher I-S fabric

45   intensities as the structural formulae of I-S approaches an end-member composition.

46

47   Keywords: Late-diagenesis; Illite-smectite; Micro-Fabric; Shale; Mudstone

48

2

49

1. Introduction

The physical, chemical and mineralogical changes which transform muds into mudstones and ultimately metamorphic pelites have been studied for many years (Sorby, 1853; Rieke and Chilingarian, 1974; Weaver, 1989; Bjørlykke and Høeg, 1997). With respect to mineralogical change, particular attention has been paid to the major reactions involving clay minerals, most obviously the transformation of smectite to illite and additional mineral changes, for example quartz and chlorite precipitation, associated with that reaction (e.g. Perry and Hower, 1970; Hower et al., 1976; Boles and Franks, 1979; Nadeau et al., 2002). Whilst X-ray diffraction has charted the mineralogical changes, Transmission Electron Microscopy (TEM) has been used to examine the microstructural and chemical changes involved not only in the smectite to illite transformation (Ahn and Peacor, 1986; Bell, 1986; Klimentidis and Mackinnon, 1986; Inoue et al., 1987a; Inoue et al., 1987b; Jiang et al., 1994; Hover et al., 1999; Masuda et al., 2001; Nadeau et al., 2002; Kim et al., 2004), but also in the reactions involved in low grade metamorphism (Merriman and Peacor, 1998; Merriman, 2002).

Other work has focused on the processes by which the initially random arrangement of phyllosilicate minerals in mud becomes organized into the highly aligned fabric observed in metapelites (Oertel and Curtis, 1972; Curtis et al., 1980; Ho et al., 1999; Jacob et al., 2000; Aplin et al., 2006; Day-Stirrat et al., 2008a; Day-Stirrat et al., 2008b). Discussion has centered on the relative roles of mechanically-driven rearrangement of particles and mineralogical changes in which neoformed phyllosilicate minerals grow normal to the principal effective stress. Whilst laboratory compaction experiments show that mechanical rearrangement of phyllosilicates is feasible (Djéran-Maigre et al., 1998; Haines et al., 2009; Voltolini et al., 2009; Day-Stirrat et al., 2011), both Ho et al. (1999) and Day-Stirrat et al. (2008a) observed a major enhancement to the

73 preferred orientation of I-S across the smectite to illite transition in the Gulf of Mexico and the

74 Podhale Basin of southern Poland, respectively. Day-Stirrat et al. (2008a) suggested that the

75 enhanced fabric intensity through the smectite to illite transition window was indicative of

76 dissolution of smectite and growth of new illite perpendicular to principal effective stress.

77   The changes in phyllosilicate fabric observed at the end of the main smectite to illite

78 transition are nevertheless substantially lower than those observed in low grade metapelites (Jacob

79 et al., 2000). This implies continuing rearrangement of fabric at temperatures and stresses higher

80 than those associated with the smectite illitization. In contact metamorphism, enhancement of

81 phyllosilicates fabrics close to the heating body have been recorded (Ho et al., 1995). In the

82 Podhale Basin (Figure 1), Day-Stirrat et al.'s (2008a) data tentatively suggested a continued

83 increase in I-S (and chlorite) fabric intensity beyond the apparent termination of the smectite to

84 illite transition or certainly the mineral reaction slowdown (Figure 2). This slowdown occurs over

85 an additional burial of 2 km and a temperature increase of 40°C (approximately 115°C to 150°C).

86 Since the porosity of these deeply buried samples is low and pore sizes are smaller than grains,

87 increases in the alignment of phyllosilicate grains are unlikely to result from mechanical processes,

88 but rather from dissolution and reprecipitation processes which may be revealed by changes in I-

89 S chemistry or microfabric. Changes in mineral chemistry have implications for density, and

90 microfabric impacts anisotropy and velocity. The practical importance of these changes is that both

91 density and velocity are key parameters in estimating both porosity and pore pressure in mud-rich

92 sequences, particularly in circumstances where sediments have been unloaded (Bowers, 1995;

93 Lahann and Swarbrick, 2011; Goulty and Sargent, 2016; Goulty et al., 2016). Since relationships

94 between vertical effective stress (VES) and porosity/density are difficult to constrain in

95 diagenetically mature samples (Yang and Aplin, 2004), an examination of the detailed chemistry

96 of mineral change in a low porosity system is timely.

97   In this study, therefore, we take some well-characterized samples from the deepest part of

98   the Podhale Basin and perform transmission electron microscopy (TEM) on both dispersed grains

99   and ion-beam thinned preparations. The TEM-EDS data allow us to look for compositional

100   changes at and beyond the smectite to illite transition, whilst lattice fringe images allow a visual

101   description of the change in crystallite morphology, thickness and fabric. The samples in this paper

102   thus represent a part of the journey a mud takes on its journey to a metamorphic pelite.

103

104   **2. Geological setting and data background**

105   The Palaeogene Podhale Basin of southern Poland is situated between the Pieniny Klippe

106   Belt to the north and the Tatra Mountains to the south (Figure 1). The basin is filled with what is

107   termed the Podhale Flysch (Olszewska and Wieczorek, 1998), deposited by submarine fans

108   (Westwalewicz-Magilska, 1986) and covering a Mesozoic basement that is exhumed in the Tatra

109   Mountains.

110   X-ray diffraction results (Table 1) on the Palaeogene mudstones (Środoń et al., 2006a)

111   describe an extremely homogeneous detrital mineral composition, with regular and clear

112   diagenetic trends with depth. Based on grain-density trends Środoń et al. (2006b) argue that two

113   wells, Chochołów PIG-1 and Bukowina Tatrzańska PIG-1, can be seen as a continuous burial

114   profile, in which a ~500m overlap produces a continuous trend in percentage of smectite in the

115   mixed-layer phase illite-smectite, as well as predictable increases in quartz and chlorite and

116   decreases in kaolinite and potassium feldspar. Present day and calculated palaeo-geothermal

117   gradients are similar in both wells (~20-25ºC km^{-1}). The overlap proposed by Środoń et al (2006b)

118   is consistent with thermal maturity data from Poprawa and Marynowski (2005). The maximum

119   burial of the Podhale Basin was achieved at ~17 Ma, based on K-Ar dates from clay mineral

120   separates from bentonites (Środoń et al., 2006b) and maximum burial was deeper than present day

121 burial. Marynowski et al. (2006) present a burial history profile through the center of the basin that

122 shows rapid Oligocene burial followed by Miocene uplift. Porosity data recorded by Day-Stirrat

123 et al. (2008a) show a consistent decrease through the established synthetic profile. The area was

124 the subject of an apatite fission track analysis by Anczkiewicz (2006), who also concluded that the

125 top of Bukowina Tatrzańska PIG-1 had previously been much deeper (totally reset tracks) than the

126 top of Chochołów PIG-1 (partially reset tracks) and subsequently it was eroded.

127   The smoothness of the diagenetic trends (Środoń et al., 2006b), the continuity of physical

128 trends in grain density (Środoń et al., 2006b), phyllosilicate preferred orientation and porosity

129 (Day-Stirrat et al., 2008a) and rapid burial and uplift (Anczkiewicz, 2006) suggest that the

130 submarine fan depositional system described by Westwalewicz-Magilska (1986) was fed by a

131 consistent source area over the period of deposition. The rapid burial of the fore-arc basin system

132 (Tari et al., 1993) of the Podhale flysch probably mitigated significant progradation of the

133 submarine fans leading to the consistent trends noted above, due to a consistent provenance.

134

135 **3. Samples and Methods**

136 **3.1 Samples**

137   The sample set consists of four fragments of cores selected from two boreholes in the

138 Podhale Basin (Figure 1): Chochołów PIG-1 in the west (samples Chochołów-06 and Chochołów-

139 60) and Bukowina Tatrzańska PIG-1 in the east (Bukowina Tatrzańska-06 and Bukowina

140 Tatrzańska-41). These samples cover a maximum temperature and depth range of ~ 50 - 150 °C

141 and 2500 – 7000 m original depth of burial (Table 1). Additional detailed sample information can

142 be found in Marynowski et al. (2006), Środoń et al. (2006b) and Day-Stirrat et al. (2008a). Sample

6

143   Chochołów-06 has 50% illite in illite-smectite whereas, Chochołów-60, Bukowina Tatrzańska-06,

144   and Bukowina Tatrzańska-41 all have 76% illite in illite-smectite.

145

146   **3.2 Transmission Electron Microscopy**

147   Chemistry of individual illite-smectite phyllosilicate particles was determined using TEM-

148   EDS; crystallite images and selected area diffraction patterns (SAED) were also obtained. Samples

149   were examined at the University of Leeds using a Philips/FEI CM200 electron microscope

150   equipped with a Field Emission Gun (FEG), and a Gatan Imaging Filter (GIF). The extinction

151   voltage was set at 3.21 kV, giving a typical energy resolution of 0.8 eV.

152   Mudstone samples were disaggregated using a gentle freeze-thaw method which does not

153   crush individual particles (Yang and Aplin, 1997). The less than 2μm fraction of the sample was

154   then separated by centrifugation. Selected < 2μm fractions were prepared for TEM-EDS by

155   dispersing 0.2 g of sample in excess ethanol. Approximately 10μL of the dilute suspension was

156   placed on a carbon coated 200-mesh copper grid and allowed to evaporate to dryness. This

157   technique assumes that phyllosilicate particles are aligned with (00l) planes approximately

158   perpendicular to the electron beam (c* parallel to beam). Care was taken to obtain SAED patterns

159   from thin grains, free from the overlap of other grains. Magnification was at 50,000x and Energy

160   Dispersive Spectra (EDS) data were acquired at between 1000 and 3000 counts per second with a

161   live time of 50 seconds using a 75Å beam diameter on the same spot as the SAED. Biotite and

162   paragonite standards were used to obtain K-factors for the transformation of intensity ratios to

163   concentrations (Cliff and Lorimer, 1975). Oxygen was not measured as it is strongly affected by

164   differences in sample thickness. Atomic concentration ratios were converted into normalized

165   mineral formulae using an anionic charge of 22 ($O_{10}[OH]_2$) and assuming that all iron occurs as

166   Fe^{3+} (Weaver, 1989; Moore and Reynolds, 1997). Oxide weight percents were calculated by

167 normalizing the atomic ratios to 95 wt% (Merriman et al., 1995). Since alkali loss, particularly

168 potassium, is a significant problem in TEM-EDS analysis (van der Pluijm et al., 1988), a consistent

169 50 second count time was used for all samples. A loss of potassium was assumed and the sodium

170 content was not included in the normalization calculations. Omitting Na^+ from the mineral formula

171 does not seriously affect interlayer charge as it comprises <0.1 cations per unit formula. All Mg^{2+}

172 and Fe^{3+} were assigned to the octahedral sheet. Estimated uncertainties in the atomic proportions

173 are: Si^{4+} and Al^{3+}, ~ ± 0.1 cations per unit formula; Fe^{3+}, Mg^{2+}, Ti^{4+}, ~ ± 0.05 cations per unit

174 formula; K^+, ~ ± 0.2 cations per unit formula (Peacor, 1992; Warren and Ransom, 1992).

175   A thin-section previously prepared for backscattered electron imaging (Day-Stirrat et al.

176 2008a) produced a sample stub that was cut 200-400μm for high resolution X-ray texture

177 goniometry (Day-Stirrat et al., 2008a). The same sample stub was prepared for lattice fringe

178 imaging with a L.R. White resin treatment (Kim et al., 1995) and was used prior to sample

179 preparation in order to prevent the collapse of smectite layers in the high vacuum environment of

180 the TEM. The preparation aimed to look at I-S in its a or b planes (c* perpendicular to beam).

181 TEM in this mode has the ability to image the size of crystallite packets and document layer

182 terminations between crystallites. Three millimeter diameter aluminum washers were attached to

183 randomly selected areas on the prepared TEM thin-section and the sample was ion-beam thinned

184 and carbon coated for TEM observation. Lattice fringe observations were obtained using a Phillips

185 CM12 Scanning Transmission Electron Microscope (STEM) at the University of Michigan. The

186 STEM was operated at an accelerating voltage of 120 kV and a beam current of ~10 nA.

187

188 **3.3 Statistical Analysis (Kolmogorov-Smirnov test)**

189   The Kolmogorov-Smirnov test (K-S Test) is a method that expresses the similarity or

190 difference between two datasets (Stuart et al., 1999). The test was used on TEM-EDS data from

191   the Podhale Basin samples. The K-S Test is non-parametric and does not require a particular

192   distribution of data (e.g. data normally distributed). It can be used on small datasets (8-13 results),

193   where simply presenting the arithmetic average of a result implies a normal distribution, and also

194   enables the K-S test a visual appraisal of the similarity of datasets. For a dataset of 20 points, the

195   test is very simple but powerful, the data are ordered and the lowest value plotted at 0.05 (1/20);

196   the second lowest value would be plotted at 0.1 (2/20), and so on up to 1 to complete the cumulative

197   distribution. Distributions can be compared visually, and a D-statistic is calculated as the

198   maximum difference or separation between two cumulative distributions and expressed as a

199   percentage.

200

201   **4. Results**

202   **4.1 Selected Area Diffraction Patterns (SAED)**

203   Morphologies of grains for which selected area diffraction patterns were obtained range

204   from euhedral crystallites (Figure 3) to subhedral crystallites (Figure 4). The associated SAED

205   patterns, taken at thin edges of crystallites, have a strong hexagonal arrangement of single crystal

206   diffraction spots in all samples. These spots correspond to (h,k,l) reflections. The presence of sharp

207   hexant reflections implies coherence between individual layers, and the absence of diffuse

208   diffraction rings is consistent with a lack of turbostratic defects.   The latter of which is

209   characteristic of smectitic interlayers.

210   Typical SAED patterns for each sample are presented in Figure 5. Chochołów-06 is the only

211   sample that deviates from the hexagonal single crystal diffraction patterns observed for

212   Chochołów-60, Bukowina Tatrzańska-06 and Bukowina Tatrzańska-41. Chochołów-06 has a

213   well-defined coherence of layers in its mixed-layer crystal particle with varying orientations of

9

214 these particles around c* (or Z) producing a slight ring effect, However, one mixed-layer crystal

215 is thick enough to define the dominant single crystal pattern.

216

217 **4.2 High resolution TEM imaging**

218 Lattice fringe images of illite and illite-smectite in samples from Bukowina Tatrzańska-

219 06 and Bukowina Tatrzańska-41 are presented in Figure 6. Bukowina Tatrzańska-06 shows thin

220 illite packets which, based on a 10Å lattice spacing, are typically around 5 layers and are situated

221 adjacent to I-S packets of similar thickness. Some I-S mixed layers show some lattice defects

222 such as layer terminations (Figure 6a), whilst others are straight crystals (Figure 6b). In

223 comparison, the samples from Bukowina Tatrzańska-41 typically reveal thicker I-S particles of

224 10-15 layers (Figure 6c and d). Here, some diagenetic crystallite packets are terminated against

225 thick illite minerals of, presumably, detrital origin. I-S crystallites show some edge dislocations

226 defined by terminations of layers of illite, probably inherited from highly imperfect, smectite

227 precursor structures. In general, the samples in Figure 6 show substantial I-S growing adjacent to

228 authigenic and detrital illite minerals. These I-S mixed layers display variable lattice

229 morphologies with some collapse structures, detailing the probable prior existence of an

230 expandable smectite component.

231

232 **4.3 Chemistry**

233 Bulk mineralogical data from Chochołów PIG-1 and Bukowina Tatrzańska PIG-1 is

234 synthesized from Środoń et al. (2006b) and Day-Stirrat et al. (2008a) (Table 1). Standard structural

235 formulae for an illite-smectite half-cell and associated elemental concentrations expressed as

236 weight percent oxides are presented in Tables 2 to 5 for Chochołów-06, Chochołów-60, Bukowina

237 Tatrzańska-06, Bukowina Tatrzańska-41, respectively. Both the octahedral totals (range = 1.92 to

10

238　2.11) and the chemical compositions are within the previously published range for illite-smectite;

239　some K^+ values are outside the range of illite, and even muscovite (>1), and are, therefore,

240　unrealistic and probably related to the noted mobility of potassium under an electron beam (Ahn

241　and Peacor, 1986; Brusewitz, 1986; Ramseyer and Boles, 1986; Środoń et al., 1986; van der Pluijm

242　et al., 1988; Weaver, 1989; Jiang et al., 1990; Li et al., 1997; Hover et al., 1999; Masuda et al.,

243　2001). The Si:Al ratio in the tetrahedral sheet is consistent with illitic material rather than pure

244　mica (Figure 7).

245　　　In order to compare the chemical composition of I-S from Chochołów-06 (50% I in I-S)

246　with that of the other samples (all 76% I in I-S), the Kolmogorov-Smirnov test is employed as

247　there are not enough data to adequately define averages by arithmetic means. Chochołów-06 has

248　a broader range of tetrahedral Si^{4+} values but includes values which are similar to or lower than

249　those in the more illitic I-S from Chochołów-60 (Figure 8a). Gulf Coast data previously published

250　by Ahn and Peacor (1986a) are presented as a reference frame for progressive illitization and

251　demonstrate the utility of the K-S test; however, it should be noted that these samples are not an

252　analog for the Podhale Basin.

253　　　The octahedral cation chemistry (Figure 8b and 8c) of Chochołów-06 displays a similar

254　range to that in the more illitic samples from Chochołów-60, albeit with more samples relatively

255　enriched in Fe^{3+} and Mg^{2+}. Total Al^{3+} is reflective of tetrahedral Si^{4+} occupancy and octahedral

256　substitution. The relative difference between sample data is described as a D-Statistic in Table 6.

257　　　I-S from Bukowina Tatrzańska-41 has a more homogeneous tetrahedral composition and a

258　much more aluminous octahedral composition than Bukowina Tatrzańska-06, which is richer in

259　Fe^{3+} (calculated Kolmogorov-Smirnov D-statistic of 43%; Figure 8f). Furthermore, the octahedral

260　composition of I-S in Bukowina Tatrzańska-41 is much more homogeneous than that in Bukowina

261　Tatrzańska-06. The D-statistic shows that all samples analyzed are statistically different in terms

262   of their octahedral cation compositions. The distributions (Figure 8) and the D-statistics (Table 6)

263   show that Bukowina Tatrzańska-41 has less Fe^{3+} and Mg^{2+} and more Al^{3+} in its octahedral sites

264   than Bukowina Tatrzańska-06.

265

266   **5. Discussion**

267   The composition of I-S reflects both that of the initial detrital supply and also changes

268   resulting from diagenesis, which ultimately transform I-S to illite, and perhaps chlorite and quartz

269   (Hower et al., 1976; Boles and Franks, 1979; Weaver, 1989; van de Kamp, 2008). From a general

270   chemical perspective, the illitization of smectite results in the export of Fe^{3+} (or Fe^{2+}) and Mg^{2+}

271   from I-S to chlorite or perhaps late-diagenetic ankerite, an increase in the concentration of Al^{3+}

272   within illite, and the formation of quartz as the more siliceous smectite is converted to illite. It is

273   commonly understood that Al^{3+} is conserved (Land et al., 1997; Land and Milliken, 2000) within

274   a diagenetic system. Whilst these general trends are well documented, they may be masked in a

275   single case by natural variations in the composition of detrital I-S related to provenance changes.

276   A common provenance and well-documented, progressive and predictable diagenetic trends

277   (Środoń et al., 2006b) makes this dataset from Podhale Basin ideal for high resolution study.

278   Furthermore, illitization of smectite has been documented to play an important role on the

279   development of an oriented alignment of neoformed clay minerals (Day-Stirrat et al., 2008a) in

280   the Podhale Basin.

281   The chemical and mineralogical data presented here show that in the deeper parts of the

282   basin (5000m to 7000m of maximum burial) the rate of smectite illitization has slowed or

283   terminated, such that the % I in I-S does not change further (Table 1). Nevertheless, detailed

284   analysis of I-S chemistry (Figure 6) and morphology (Figure 8) suggests continued

285   recrystallization with increasing depth, observed as an increase in the size and coherency of I-S

286 crystallite packets. In terms of the use of sonic velocity as a method to estimate porosity and pore

287 pressure, the implication of increased preferred orientation and thicker, more coherent I-S packets

288 is increased velocities at a constant porosity and pore fluid pressure.

289 Further, with increasing burial depth, K_2O in the whole rock (Środoń et al., 2006b) is

290 approximately conserved (Table 1). By assuming that K-feldspar contains 15% K^+ in its structural

291 formula (i.e. 0.1 Na per formula: Środoń, 2009) and assigning an appropriate percentage of the

292 K_2O to K-feldspar, the rest of the K_2O can be assigned to K-bearing 2:1 clays (mica, illite and

293 illite-smectite; Table 1). These calculations show that the K_2O content of the 2:1 clay fraction does

294 not evolve down the profile, staying between 5.6 and 7.4%. This consistency, despite a clear

295 smectite illitization trend, can be explained only by a redistribution of K_2O within the 2:1 fraction

296 (dissolution of detrital illite/mica providing K_2O for neoformed illite). Dissolution of illite with

297 increasing burial depth is probably unreasonable as illite would be in equilibrium with smectite

298 illitization.

299 It is well known that smectite produces concentric ring patterns in SAED associated with

300 turbostratic disorder (Moore and Reynolds, 1997), resulting from the weak mutual attraction

301 between hydrated cations in the interlayer space and adjacent 2:1 layers and the resultant lack of

302 'keying' effects which allows more random layer positioning. XRD indicates that the most

303 diagenetically immature sample in this study contains randomly interstratified (R0) I-S with 50%

304 illite layers (Środoń et al., 2006b), but only limited turbostratic disorder (Figure 5). The nature of

305 the smectite and illite interfaces in interstratified mixed-layered 'crystallite packets' can affect

306 SAED patterns (Bell, 1986), as the boundary between smectite and illite layers may be layer

307 terminating, changing the crystal lattice planes on the scale of the electron beam and producing

308 what appears to be small amounts of turbostratic disorder (see Figure 5). The three more

309 diagenetically mature samples contain R1 ordered I-S (Środoń et al., 2006b) with essentially

310   identical (76%) proportions of I in I-S; these samples have correspondingly similar SAED patterns

311   which are also similar to those observed in previous studies of similar material (e.g. Ahn and

312   Peacor, 1986; Jiang et al., 1990). However, the ordering suggested by XRD is not entirely matched

313   by the high resolution TEM observations, which show progressive ordering from Bukowina

314   Tatrzańska-06 to Bukowina Tatrzańska-41 and an increase in crystallite size. This suggests that I-

315   S continues to recrystallize beyond the level implied by XRD data, revealed by TEM because this

316   technique can discern a packet of crystallites within a size fraction, whereas XRD is the average

317   crystallographic response of all the crystallites in that fraction. Small differences in SAED patterns

318   of the three more mature samples most probably relate to (a) the coherency of 'crystallite packets',

319   with larger packets producing more clearly identified single crystal patterns (Ahn and Peacor,

320   1986; Li et al., 1997), and (b) the octahedral substitution of Fe^{3+} (or Fe^{2+}) and Mg^{2+} for Al^{3+} in the

321   octahedral layer, with Fe^{3+} being the most significant substitution due to the size of the atom

322   relative to Al^{3+}. The most coherent SAED patterns for I-S are thus seen in Bukowina Tatrzańska-

323   41, which contain, according to lattice fringe images (Figure 6), the thickest I-S crystallites which

324   also have the least Fe^{3+} and Mg^{2+} in the octahedral sheet (Figure 8).

325   It has been previously shown that on a $1mm^2$ scale, the preferred orientation of I-S

326   crystallites (Figure 2) in these wells increases substantially during the main phase of illitization

327   (Day-Stirrat et al., 2008a); a similar phenomenon was observed in the Gulf of Mexico by Ho et

328   al. (1999). The change in preferred orientation implies that illitization occurs as a dissolution –

329   reprecipitation reaction and that the neoformed mineral grows perpendicular to maximum

330   effective stress (Day-Stirrat et al., 2008a). In the closed system implied by the whole rock

331   chemistry (constant K_2O) and mineralogy of these mudstones (Środoń et al., 2006b), potassium

332   for illite is supplied from K-feldspar, with additional Al^{3+} and Si^{4+} from kaolinite. Changes in the

333   proportion of illite in mixed-layer I-S halt at around 5 km paleo burial depth that is around 100°C

334   (Table 1, Figure 2). More deeply buried samples, such as Bukowina Tatrzańska-41, which has a

335   maximum burial depth of 7.1 km and a maximum paleo-temperature of close to 150°C (Środoń

336   et al., 2006a), have essentially identical % I in I-S. However, in the apparent absence of % I in I-

337   S change, the preferred orientation of I-S in the more deeply buried samples is somewhat higher.

338   These data could imply (a) mechanical rearrangement of phyllosilicates as a result of higher

339   effective stresses; (b) continued recrystallization but with no change in % I within I-S; (c)

340   formation of a variably aligned phyllosilicate fabric during the main phase of illitization, with no

341   further recrystallisation during continued burial.

342   It is highly unlikely that the somewhat enhanced preferred orientation is due to

343   mechanical rearrangement. Firstly, the samples have low porosities and secondly, mercury

344   injection porosimetry data suggest that most pores are smaller than ~ 20 nm (Day-Stirrat et al.,

345   2008a). The lack of physical space precludes substantial mechanical reorientation of particles

346   which are larger than the pores. Given that the diagenetic system here appears to be closed, any

347   change in the microfabric is likely to result in a shift of load from matrix grains to pore fluid,a

348   decrease in effective stress, an argument recently discussed by Goulty et al. (2016). Given that

349   the pore volume to matrix volume is weighed heavily in favor of the matrix, any change could

350   have proportionally large effects on pore fluid. Therefore, in high pressure high temperature

351   wells the loading-unloading behavior (Bowers, 1995), decrease in effective stress, may be

352   extremely complex and potentially away from illite compaction trends defined for lower

353   effective stresses (Lahann, 2002; Lahann and Swarbrick, 2011).

354   Unfortunately, our data cannot unequivocally differentiate hypotheses (b) and (c).

355   However, lattice fringe images suggest that I-S crystallite packages in Bukowina Tatrzańska-41

356   are larger than those in Bukowina Tatrzańska-06, implying continuing crystal growth without the

357   destruction of smectite layers in mixed-layer I-S (Figure 6). We infer that the I-S does not

358 become more illitic due to a lack of supply of K^+, or that residual smectite layers are physically

359 occluded from interacting with cations in solution. A clear compositional difference (Figure 8)

360 between I-S in Bukowina Tatrzańska-06 and Bukowina Tatrzańska-41 supports the idea of

361 continued recrystallization. The octahedral occupancy of I-S in Bukowina Tatrzańska-41 is much

362 more aluminous than that of Bukowina Tatrzańska-06, essentially more mica like, and the

363 overall composition of I-S in Bukowina Tatrzańska-41 is much more homogeneous than that in

364 Bukowina Tatrzańska-06. Stated very simply, Bukowina Tatrzańska-41 has a distribution of

365 illite-smectite chemical formulae that are simplified relative to Bukowina Tatrzańska-06,

366 consistent with the progressive conversion of illite towards a 'mica' at significantly greater

367 temperatures (van de Kamp, 2008).

368   The data in this study, plus those from Środoń et al. (2006b) and Day-Stirrat et al.

369 (2008a), indicate continued recrystallization and export of Fe^{3+} from I-S as, during late

370 diagenesis, it transforms towards a more muscovite-like composition. We propose that this is

371 part of a series of diagenetic steps (Figure 9) that converts a broadly isotropic fabric inherited as

372 a result of the deposition of clay floccules to the highly aligned fabric observed in low grade

373 metamorphic pelites (Haines et al., 2009). Reorientation of the clay fabric is restricted during the

374 main stage of mechanical compaction, during which water is expelled, but is enhanced during the

375 main stage of smectite illitization. In this study, at higher levels of diagenesis, we see that whilst

376 recrystallization of illite continues, there is a limited change in the orientation of the illite fabric.

377 As diagenesis gives way to low grade metamorphism, there is once again a more striking

378 development of an aligned phyllosilicate fabric, reflecting continuing clay mineral

379 recrystallization and growth (Figure 9). Abrupt diagenetic steps are not applicable to all major

380 diagenetic reactions. For example, once quartz cementation reaches a kinetically favorable

16

381   activation energy (with the presence of a clean quartz surface) and temperature the reaction

382   simply runs until there is no more space for quartz cementation (Taylor et al., 2010).

383

384   **6. Conclusions**

385   TEM-EDS data and statistical tests presented here describe a systematic change in I-S

386   chemistry with increased burial temperature beyond the termination of the smectite to illite

387   transformation. TEM-EDS data is accompanied by SAED patterns that show well defined

388   coherence of layers in I-S packets, single crystal patterns and an absence of turbostratic disorder.

389   Concomitant with this change in mineral formulae is an increase in crystallinity observable in

390   lattice fringe images and a change from high angle contacts between discrete I-S packets to more

391   coalesced crystallites. We propose that the data presented here describe the continued increase in

392   the preferred orientation of I-S beyond the smectite to illite transformation. This involves a change

393   in crystallite chemistry reflected by (a) the progressive removal of Fe^{3+} and Mg^{2+} from the

394   octahedral sheet of I-S, (b) a decrease in crystallite layer rotation and (c) the coalescence of I-S

395   crystallites in a high effective stress regime. We suggest that these relatively subtle changes are

396   one of a series of diagenetic steps which convert chemically diverse I-S with a broadly isotropic

397   phyllosilicate fabric into chemically homogeneous illite with a highly anisotropic fabric in low

398   grade metamorphic rocks. These results have implications for loading-unloading trends in

399   diagenetically mature siliciclastic systems and for predicating porosity and pore pressure from

400   wireline logs.

405 Table 1 Present day depth [m], maximum burial depth [m], %I in I-S and bulk mineralogy from X-ray diffraction
406 (Środoń et al., 2006b).

Sample	Chl-4	Chl-6	Chl-12	Chl-20	Chl-23	Chl-28	Chl-38	Chl-44	Chl-56	Chl-60	Chl-66
Actual Burial Depth (m)	193	280	514	821	1031	1283	1671	2012	2410	2611	2968
Estimated Maximum Burial Depth [m]	2393	2480	2714	3021	3231	3483	3871	4212	4610	4811	5168
Max. Temp (°C) from modeling	57.5	60	67.5	75	80	85	95	105	115	120	127.5
Quartz	19.0	24.3	18.5	22.9	21.7	20.4	16.3	26.0	20.5	27.5	22.4
K-Feldspar	2.2	2.3	2.2	1.5	1.3	0.5	1.5	1.0	0.5	0.4	0.5
Plagioclase	3.0	5.9	3.7	4.7	3.6	5.7	5.0	7.0	6.5	9.0	6.0
Calcite	7.7	10.2	11.9	10.5	10.0	10.4	0.9	3.7	3.6	13.2	17.0
Dolomite	3.8	5.4	3.5	4.1	4.5	4.7	4.5	6.2	5.2	4.6	6.7
Halite	0.0	0.0	0.0	0.0	0.0	0.0	0.6	0.5	1.2	0.0	0.0
Pyrite	1.5	1.5	1.2	0.7	0.9	2.3	2.3	2.5	1.8	1.2	1.5
Siderite	0.0	0.4	0.3	0.7	0.8	0.0	0.0	0.2	0.0	0.2	0.2
Anatase	0.0	0.0	0.0	0.0	0.2	0.0	0.6	0.4	0.5	0.7	0.5
Kaolinite	3.2	1.5	3.2	3.6	2.9	2.6	1.0	1.0	0.8	0.0	0.0
Illite + Mica + Fe-Smectite	45.8	46.8	50.2	49.2	43.9	49.1	60.8	53.9	60.1	41.1	41.8
Chlorite	0.7	4.0	2.6	2.1	2.6	3.6	7.4	5.2	4.8	4.7	4.2
Total clay	49.7	52.3	56.0	54.9	49.4	55.3	69.2	60.1	65.7	45.8	46.0
%S in I/S	52	50	63	47	45	44	24	32	27	24	31
Ordering	0	0	0	0	0/1	0/1	1	1	1	1	1
K2O (%)	3.6	3.6	3.2	3.0	2.9	3.0	4.7	3.4	4.2	2.9	2.9
K-Bearing 2:1 clays	22.0	23.4	18.6	26.1	24.1	27.5	46.2	36.7	43.9	31.2	28.8
K2O in Illite Wt.%	2.4	2.3	2.2	2.3	2.3	2.8	3.6	2.9	3.9	2.7	2.7
% K2O in Illite	9.1	10.0	8.6	11.4	10.3	9.9	12.7	12.7	11.2	11.5	10.8
K2O/K-Feldspar	1.6	1.5	1.5	2.0	2.2	6.0	3.1	3.4	8.5	7.3	5.8
TEM Study Samples And %I in I-S		Chl-6 50%								Chl-60 76%	

Sample	BkT-1	BkT-6	BkT-12	BkT-17	BkT-23	BkT-28	BkT-35	BkT-41
Actual Burial Depth (m)	102	294	611	903	1261	1595	1904	2201
Estimated Maximum Burial Depth [m]	4908	5100	5417	5709	6067	6401	6710	7007
Max. Temp (°C) from modeling	103	107	114	120	127	134	141	147
Quartz	26.6	25.2	27.0	24.1	23.3	27.0	29.4	26.4
K-Feldspar	0.8	0.5	1.0	0.5	1.0	0.0	0.5	0.0
Plagioclase	7.1	6.8	6.6	5.3	4.5	6.2	6.3	5.7
Calcite	9.5	7.3	5.4	6.9	6.1	11.2	0.8	8.8
Dolomite	7.5	6.5	7.6	6.9	7.8	5.5	6.2	4.2
Halite	0.0	0.0	0.0	0.5	0.0	0.0	0.5	1.0
Pyrite	0.9	0.9	1.2	1.3	1.0	1.5	2.4	3.0
Siderite	0.0	0.5	0.0	0.0	0.0	0.0	0.0	0.0
Anatase	0.5	0.5	0.5	0.5	0.4	0.4	0.5	0.3
Kaolinite	0.8	0.5	0.0	0.0	0.0	0.0	0.0	0.0
Illite + Mica + Fe-Smectite	53.6	54.3	52.0	48.1	50.7	46.8	50.1	51.5
Chlorite	5.6	5.6	6.1	3.1	4.2	4.4	3.6	4.0
Total clay	60.0	60.4	58.1	51.2	54.9	51.2	53.7	55.5
%S in I/S	25	24	26	25	20	30	18	24
Ordering	1	1	1	1	1	1	1	1
K2O (%)	3.5	3.6	3.1	3.3	3.3	3.1	3.4	3.3
K-Bearing 2:1 clays	40.2	41.3	38.5	36.1	40.6	32.8	41.1	39.1
K2O in Illite Wt.%	3.1	3.3	2.6	3.1	2.8	3.1	3.1	3.3
% K2O in Illite	13.1	12.6	14.6	11.8	14.5	10.6	13.1	11.9
K2O/K-Feldspar	4.4	7.1	3.1	6.6	3.3		6.8	
TEM Study Samples And %I in I-S		BkT-6 76%						BkT-41 76%

407
408
409
410
411
412

413
414 Table 2: Chochołów-06 structural formulae for a half cell and associated elemental concentrations expressed as wt.%
415 oxides normalized to 95%.(Merriman et al., 1995), 50 % illite in illite-smectite.

	E001	E003	E005	E009	E011	E019
Si	3.31	3.65	3.12	3.56	3.12	3.59
Al	0.69	0.35	0.88	0.44	0.88	0.41
Tet. Sum	4.00	4.00	4.00	4.00	4.00	4.00
Al	1.93	1.77	1.47	1.59	1.73	1.61
Fe	0.07	0.07	0.20	0.14	0.07	0.15
Mg	0.00	0.10	0.23	0.28	0.19	0.20
Ti	0.01	0.02	0.02	0.00	0.03	0.00
Oct. Sum	2.01	1.96	1.92	2.01	2.02	1.96
Ca	0.00	0.02	0.00	0.02	0.01	0.03
K	0.68	0.52	1.34	0.66	0.95	0.67
Inter. Sum	0.68	0.54	1.34	0.68	0.96	0.70
SiO_2	50.24	57.21	44.78	54.52	46.67	0.69
Al_2O_3	33.77	28.18	28.50	26.23	33.08	33.08
TiO_2	0.17	0.47	0.41	0.35	0.69	0.15
Fe_2O_3	1.37	1.46	3.72	2.88	1.37	11.15
MgO	1.24	1.01	2.24	2.88	1.88	46.67
CaO	0.16	0.24	0.33	0.28	0.15	1.88
K_2O	8.05	6.43	15.04	7.86	11.15	1.37
Total	95	95	95	95	95	95

	E021	E024	E026	E028	E030
Si	3.50	3.44	3.32	3.26	3.04
Al	0.50	0.56	0.68	0.74	0.96
Tet. Sum	4.00	4.00	4.00	4.00	4.00
Al	1.48	1.63	1.62	1.69	1.55
Fe	0.24	0.18	0.15	0.19	0.20
Mg	0.25	0.16	0.14	0.09	0.33
Ti	0.03	0.02	0.01	0.03	0.02
Oct. Sum	2.00	1.99	1.92	2.00	2.10
Ca	0.19	0.02	0.25	0.01	0.09
K	0.34	0.66	0.55	0.76	0.82
Inter. Sum	0.53	0.68	0.80	0.77	0.91
SiO_2	54.05	52.54	50.58	49.26	45.07
Al_2O_3	25.88	28.45	29.69	31.16	31.59
TiO_2	0.63	0.49	0.15	0.59	0.36
Fe_2O_3	5.02	3.64	3.12	3.89	3.85
MgO	2.57	1.62	1.39	0.92	3.27
CaO	2.72	0.34	3.54	0.16	1.31
K_2O	4.14	7.91	6.53	9.02	9.56
Total	95	95	95	95	95

19

416 Table 3: Chochołów-60 structural formulae for a half cell and associated elemental concentrations expressed as wt.%
417 oxides normalized to 95%.(Merriman et al., 1995), 76 % illite in illite-smectite.

	J001	J009	J011	J013	J015	J017	J019	J021
Si	3.32	3.28	3.47	3.37	3.25	3.12	3.19	3.37
Al	0.68	0.72	0.53	0.63	0.75	0.88	0.81	0.63
Tet. Sum	4.00	4.00	4.00	4.00	4.00	4.00	4.00	4.00
Al	1.81	1.78	1.53	1.80	1.67	1.45	1.72	1.93
Fe	0.10	0.14	0.17	0.08	0.16	0.21	0.17	0.10
Mg	0.14	0.07	0.21	0.05	0.10	0.31	0.01	0.01
Ti	0.02	0.01	0.03	0.01	0.05	0.02	0.02	0.01
Oct. Sum	2.07	2.00	1.94	1.94	1.98	1.99	1.92	2.05
Ca	0.05	0.07	0.11	0.07	0.06	0.05	0.09	0.04
K	0.49	0.62	0.65	0.70	0.76	1.13	0.89	0.45
Inter. Sum	0.54	0.69	0.76	0.77	0.82	1.18	0.98	0.49
SiO_2	51.62	50.26	52.81	51.63	49.02	45.41	47.59	52.78
Al_2O_3	32.71	32.45	26.64	31.63	31.04	28.69	32.11	33.99
TiO_2	0.48	0.23	0.62	0.26	0.92	0.33	0.32	0.12
Fe_2O_3	2.00	2.94	3.42	1.59	3.16	3.99	3.28	2.05
MgO	1.48	0.76	2.19	0.53	1.00	3.07	0.08	0.06
CaO	0.77	0.95	1.54	0.96	0.84	0.67	1.20	0.52
K_2O	5.94	7.42	7.79	8.41	9.02	12.84	10.42	5.48
Total	95	95	95	95	95	95	95	95

418
419
420
421
422
423
424
425
426
427
428
429
430
431
432
433
434
435
436
437
438
439
440
441
442
443
444

445 Table 4: Bukowina Tatrzańska-06 structural formulae for a half cell and associated elemental concentrations expressed
446 as wt.% oxides normalized to 95%.(Merriman et al., 1995), 76 % illite in illite-smectite.

	H003	*H007*	*H009*	*H011*	*H013*	*H018*	*H022*
Si	3.36	3.22	3.38	3.52	3.32	3.42	3.26
Al	0.64	0.78	0.62	0.48	0.68	0.58	0.74
Tet. Sum	4.00	4.00	4.00	4.00	4.00	4.00	4.00
Al	1.66	1.32	1.68	1.66	1.76	1.76	1.72
Fe	0.20	0.34	0.18	0.12	0.14	0.07	0.14
Mg	0.22	0.28	0.03	0.16	0.07	0.17	0.05
Ti	0.00	0.02	0.01	0.00	0.01	0.01	0.01
Oct. Sum	2.08	1.96	1.90	1.94	1.98	2.01	1.92
Ca	0.19	0.00	0.03	0.04	0.00	0.01	0.06
K	0.22	1.18	0.91	0.73	0.80	0.71	0.89
Inter. Sum	0.41	1.18	0.94	0.77	0.80	0.72	0.95
SiO_2	52.40	46.43	50.66	53.39	50.30	52.61	48.84
Al_2O_3	30.52	25.62	29.21	27.60	31.49	30.38	31.35
TiO_2	0.03	0.32	0.16	0.53	0.21	0.25	0.28
Fe_2O_3	4.19	6.50	3.54	2.50	2.76	1.34	2.84
MgO	2.31	2.70	0.30	1.61	0.71	1.73	0.49
CaO	2.81	0.04	0.41	0.63	0.01	0.14	0.78
K_2O	2.75	13.39	10.71	8.75	9.51	8.55	10.42
Total	95	95	95	95	95	95	95
	H024	*H026*	*H028*	*H030*	*H032*	*H034*	
Si	3.17	3.39	3.07	3.39	3.10	3.46	
Al	0.83	0.61	0.93	0.61	0.90	0.54	
Tet. Sum	4.00	4.00	4.00	4.00	4.00	4.00	
Al	1.49	1.54	1.04	1.58	1.44	1.53	
Fe	0.22	0.26	0.56	0.19	0.22	0.15	
Mg	0.24	0.15	0.29	0.16	0.31	0.23	
Ti	0.00	0.05	0.06	0.02	0.05	0.02	
Oct. Sum	1.95	2.00	1.95	1.95	2.02	1.93	
Ca	0.10	0.07	0.22	0.01	0.04	0.00	
K	1.01	0.55	0.89	0.90	1.02	0.94	
Inter. Sum	1.11	0.62	1.11	0.91	1.06	0.94	
SiO_2	46.54	51.70	43.80	50.73	45.44	51.93	
Al_2O_3	28.87	27.72	23.78	27.82	28.98	26.28	
TiO_2	0.00	1.08	1.05	0.36	0.97	0.43	
Fe_2O_3	4.28	5.36	10.67	3.88	4.34	2.94	
MgO	2.38	1.55	2.77	1.56	3.01	2.36	
CaO	1.30	0.96	2.95	0.14	0.53	0.07	
K_2O	11.63	6.63	9.98	10.52	11.72	10.99	
Total	95	95	95	95	95	95	

447

448 Table 5: Bukowina Tatrzańska-41 structural formulae for a half cell and associated elemental concentrations expressed
449 as wt.% oxides normalized to 95% (Merriman et al., 1995). 76 % illite in illite-smectite.

	C003	C005	C007	C010	C012	C014	C016	C018
Si	3.28	3.24	3.22	3.52	3.38	3.28	3.47	3.40
Al	0.72	0.76	0.78	0.48	0.62	0.72	0.53	0.60
Tet. Sum	4.00	4.00	4.00	4.00	4.00	4.00	4.00	4.00
Al	1.77	1.88	1.94	1.50	1.76	1.79	1.58	1.62
Fe	0.11	0.04	0.07	0.07	0.10	0.09	0.17	0.14
Mg	0.19	0.00	0.10	0.35	0.18	0.02	0.13	0.19
Ti	0.01	0.01	0.00	0.07	0.02	0.01	0.03	0.03
Oct. Sum	2.08	1.93	2.11	1.99	2.06	1.91	1.91	1.98
Ca	0.00	0.10	0.03	0.16	0.00	0.00	0.02	0.00
K	0.67	0.75	0.47	0.45	0.58	0.97	0.86	0.82
Inter. Sum	0.67	0.85	0.50	0.61	0.58	0.97	0.88	0.82
SiO_2	49.83	49.19	50.14	54.44	52.31	49.30	52.21	51.39
Al_2O_3	32.18	34.07	35.93	26.10	31.27	31.95	27.07	28.55
TiO_2	0.19	0.26	0.11	1.41	0.35	0.23	0.66	0.69
Fe_2O_3	2.27	0.81	1.52	1.52	2.13	1.88	3.40	2.75
MgO	1.94	0.27	1.00	3.64	1.90	0.16	1.27	1.91
CaO	0.63	1.43	0.50	2.38	0.05	0.02	0.23	0.01
K_2O	7.96	8.97	5.79	5.52	6.99	11.45	10.17	9.69
Total	95	95	95	95	95	95	95	95

450
451
452
453
454
455
456
457
458
459
460
461
462
463
464
465
466
467
468
469
470
471
472
473
474
475
476

477 Table 6. Summary of the difference using the Kolmogorov-Smirnov test between samples in the Podhale Basin
478 (ND=no data).

Well and Sample	Difference in Fabric Intensity [m.r.d.]	Difference in % I in I-S	Difference in Octahedral Fe D-Statistic	Difference in Octahedral Mg D-Statistic	Difference in Total Al D-Statistic	Difference in Tetrahedral Si D-Statistic
20% I in I-S and 80% I in I-S (Ahn and Peacor, 1986)	ND	60	75	76	88	100
Chochołów-06 and Chochołów-60	1.48	26	45	40	28	30
Bukowina Tatrzańska-06 and Bukowina Tatrzańska-41	1.2	0	43	30	18	18
Chochołów-06 and Bukowina Tatrzańska-06	0.25	26	37	10	5	8
Chochołów-06 and Bukowina Tatrzańska-41	2.53	26	50	27	18	25
Chochołów-60 and Bukowina Tatrzańska-06	0.32	0	40	48	23	27
Chochołów-60 and Bukowina Tatrzańska-41	0.95	0	39	23	4	25

479
480
481
482
483
484
485
486
487
488
489
490
491
492
493
494
495
496
497
498
499
500
501
502
503
504
505
506
507
508

509

510
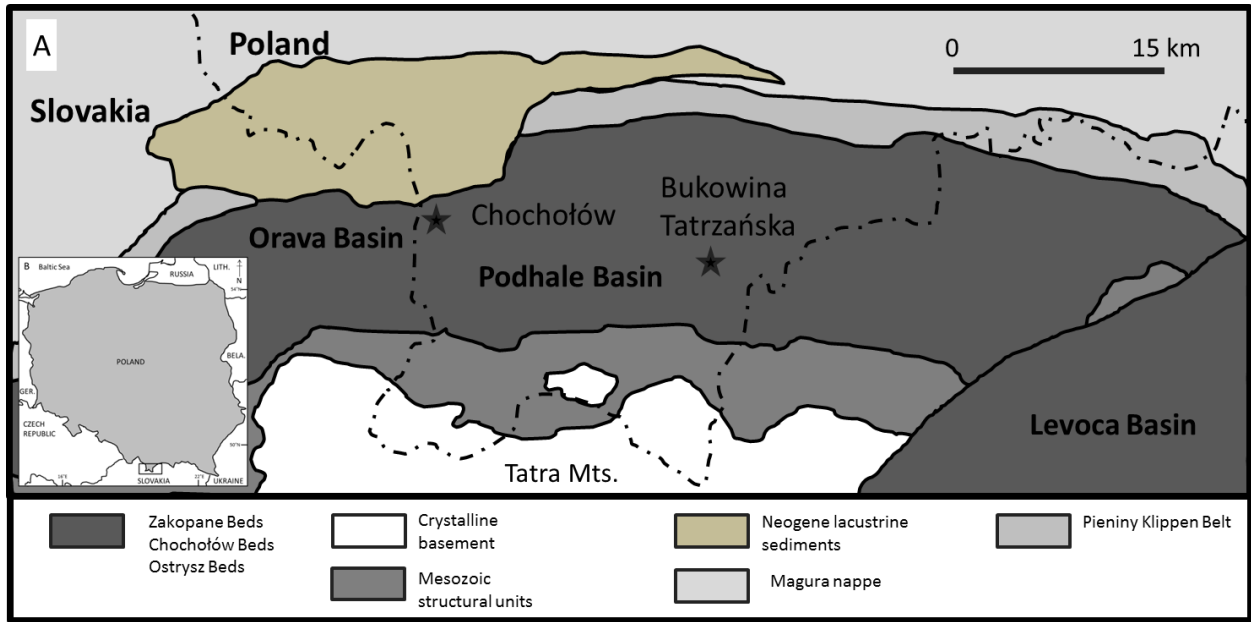
Figure 1. A: The Podhale Basin with its surrounding sub-basins. and the locations of the Chochołów PIG-1 and
Bukowina Tatrzańska PIG-1 wells (adapted from Środoń et al., 2006b).

513
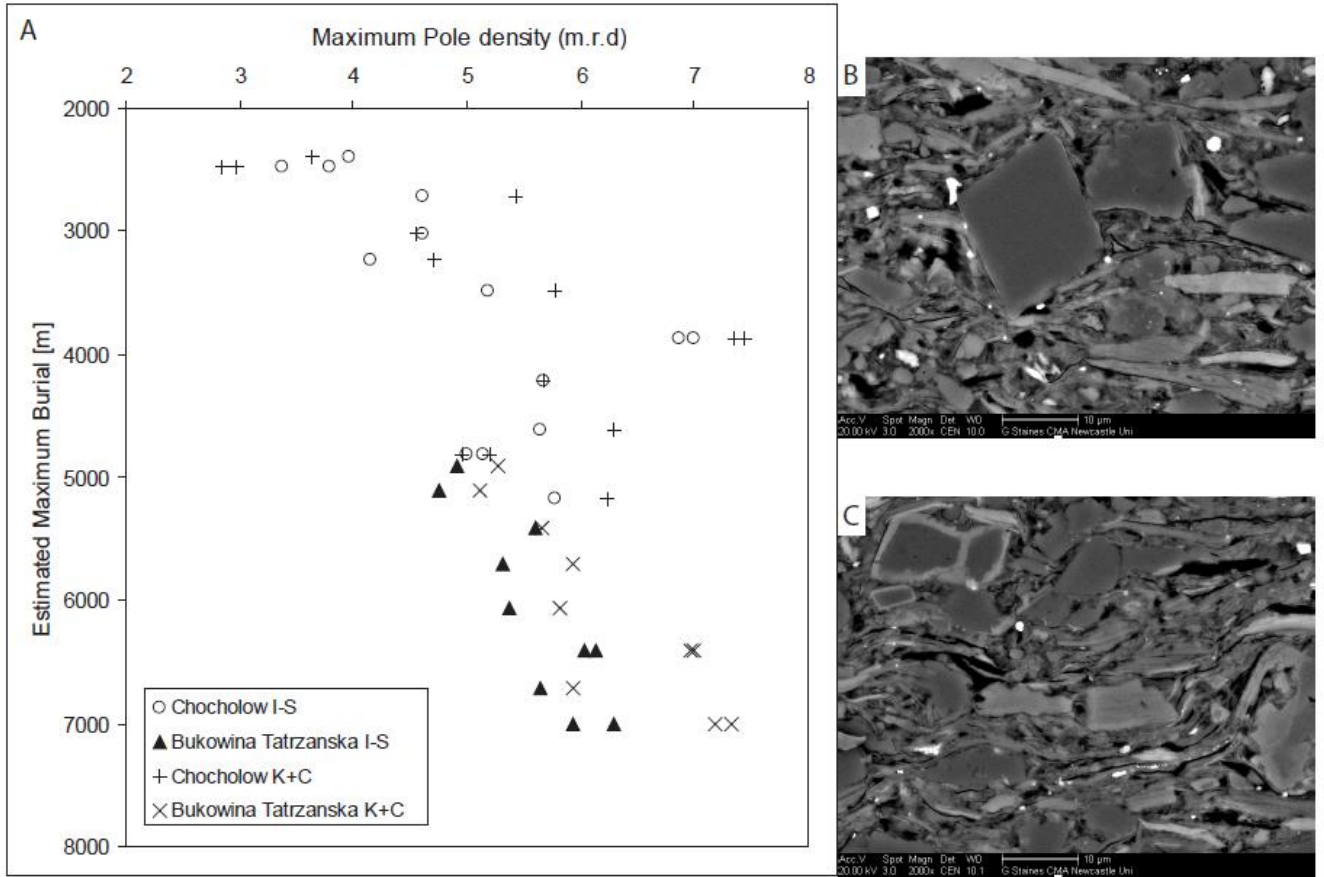
514
515 Figure 2. (A) Maximum pole density (m.r.d.) for illite-smectite and kaolinite + chlorite for samples from the Podhale
516 Basin (Day-Stirrat et al, 2008a). Backscattered electron images (B) and (C) of samples at 2480m and 4610m (see Day-
517 Stirrat et al, 2008a for more images). Smectite illitization appears to terminate at around 4500 m of maximum burial.
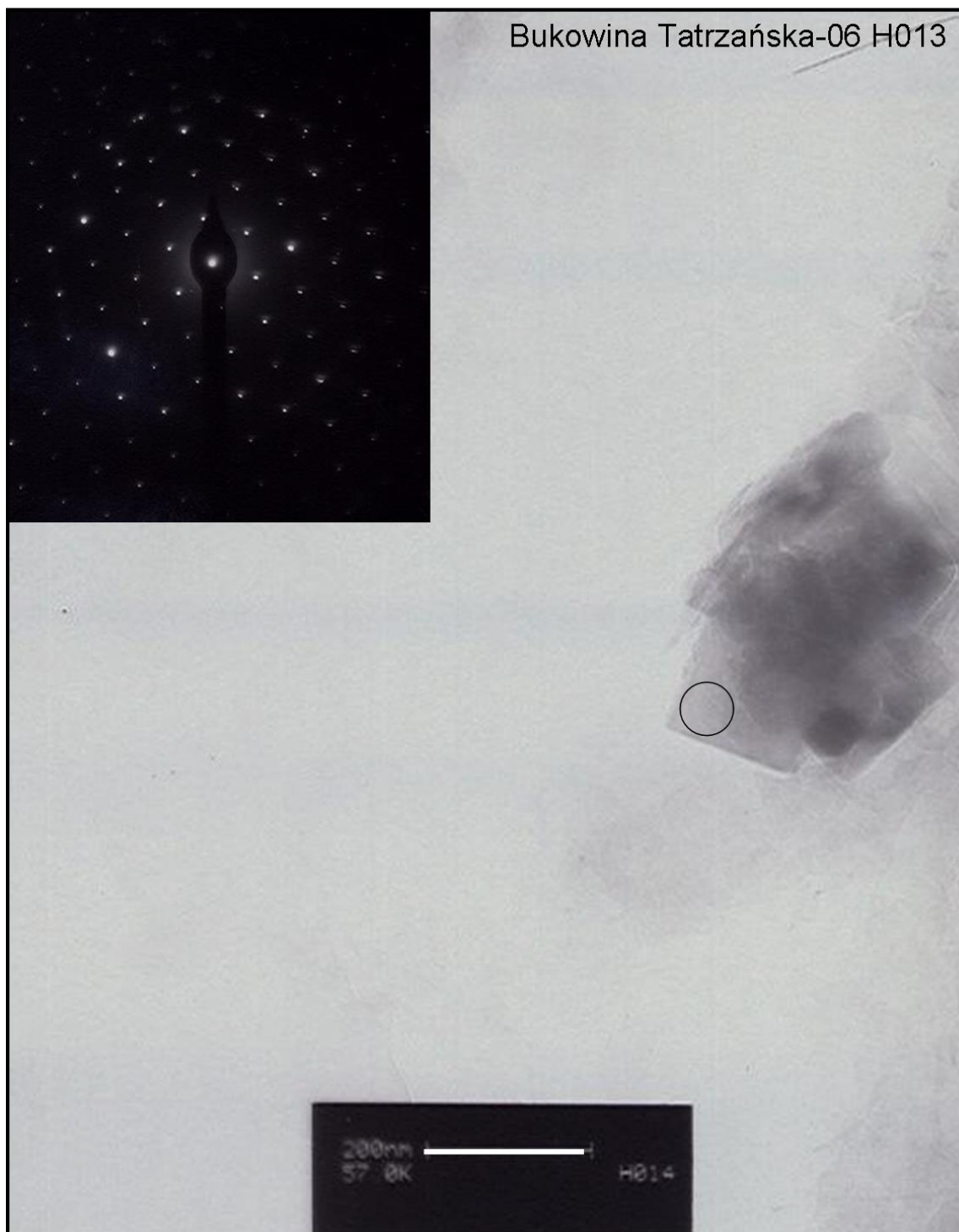
Figure 3. Sample Bukowina Tatrzańska-06 H013 (TEM-EDS data in Table 4). Euhedral grain drop-cast on a carbon film-supported 200-mesh copper grid with c* (Z) parallel to the electron beam. The scale bar is 200nm and the location of diffraction aperture is schematically noted by the ring. The Selected Area Diffraction Pattern (inset) shows a strong hexanet of discrete spots free from distortions or rings that are indicative of turbostratic layering.
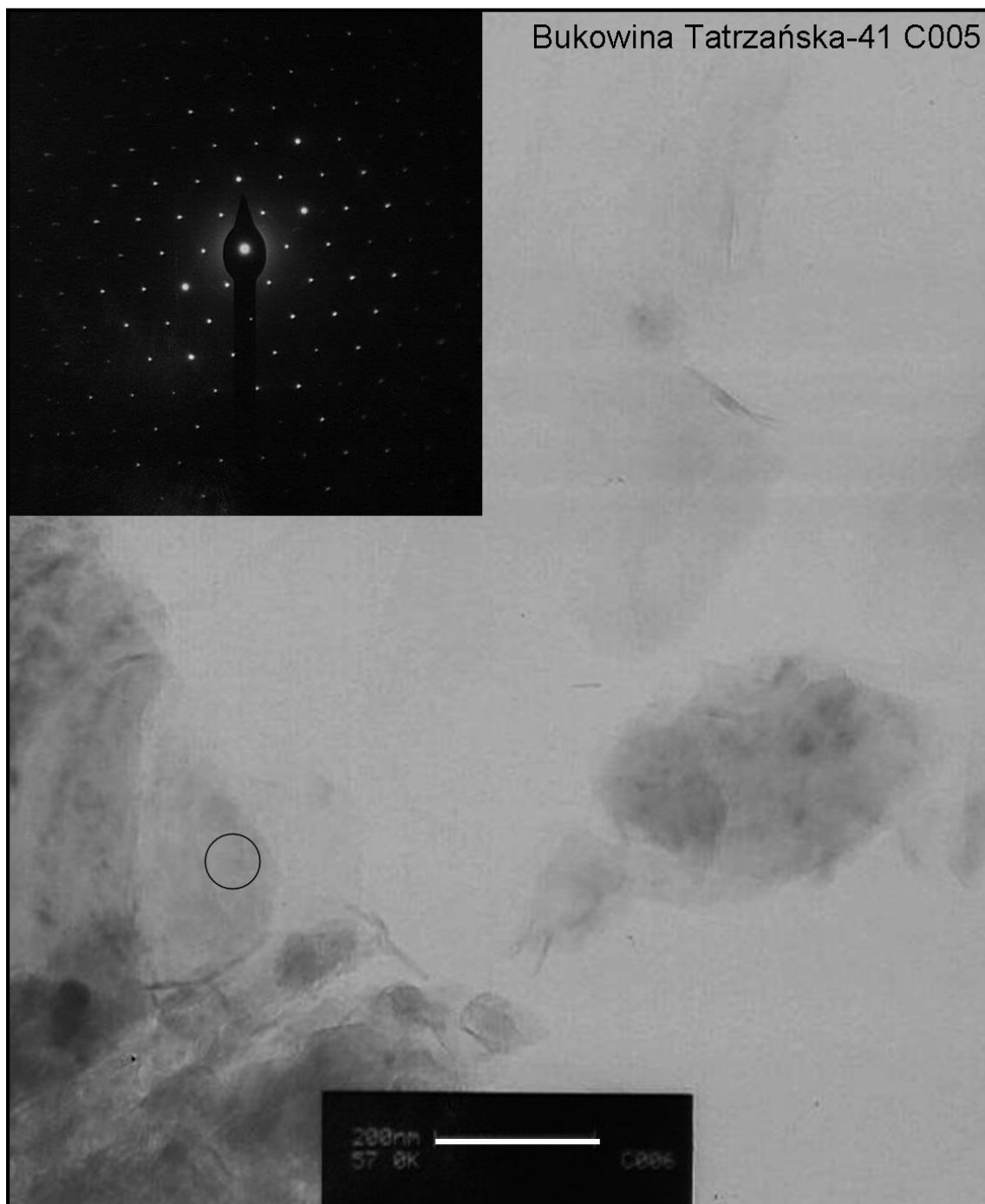
Figure 4. A grain in sample Bukowina Tatrzańska-41 C005 (TEM-EDS data in Table 5). Grain drop-cast on a carbon film-supported 200-mesh copper grid with c* (Z) parallel to the electron beam. The scale bar is 200nm and the location of diffraction aperture is schematically noted by the ring. The Selected Area Diffraction Pattern (inset) shows a strong hexanet of discrete spots free from distortions or rings that are indicative of turbostratic layering.

27
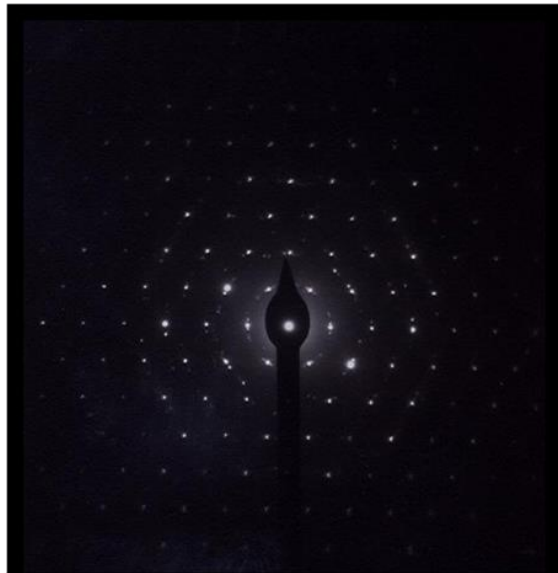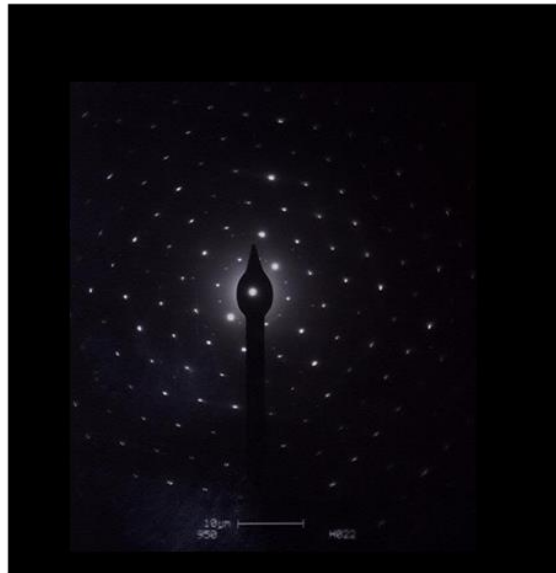
Chochołów-06 E026

Bukowina Tatrzańska-06 H022
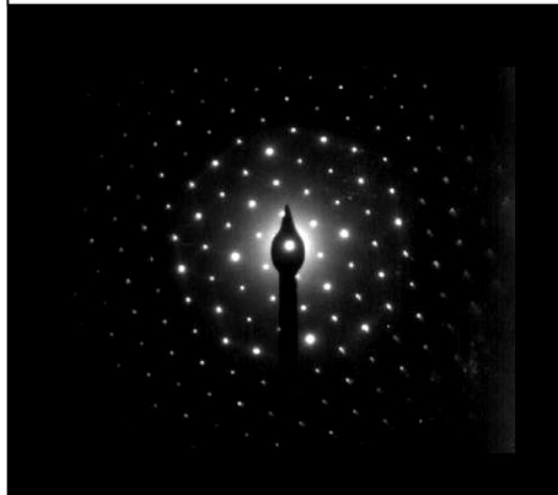
Chochołów-60 J011
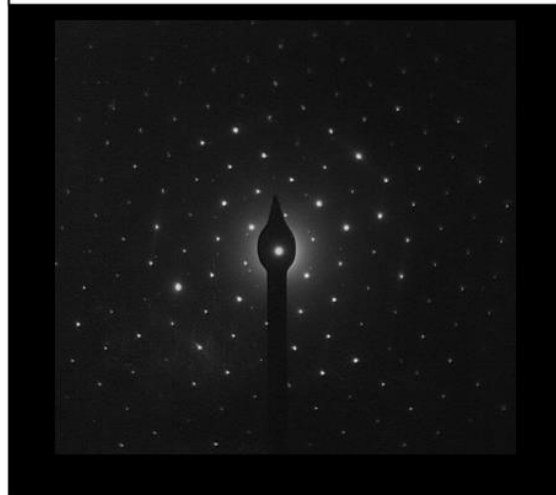
Bukowina Tatrzańska-41 C014

Figure 5. Representative Selected Area Diffraction Patterns for samples Chochołów-06, Chochołów-60, Bukowina Tatrzańska-06 and Bukowina Tatrzańska-41 (Tables 2, 3, 4 and 5 for mineral formulae). Chochołów-06 shows well defined coherence of layers in packets with varying orientations, but with one packet that is thick enough to produce a hexagonal single crystal pattern. Chochołów-60, Bukowina Tatrzańska-06 and Bukowina Tatrzańska-41 have Selected Area Diffraction Patterns for ($h,k,0$) showing well-defined single crystal patterns.
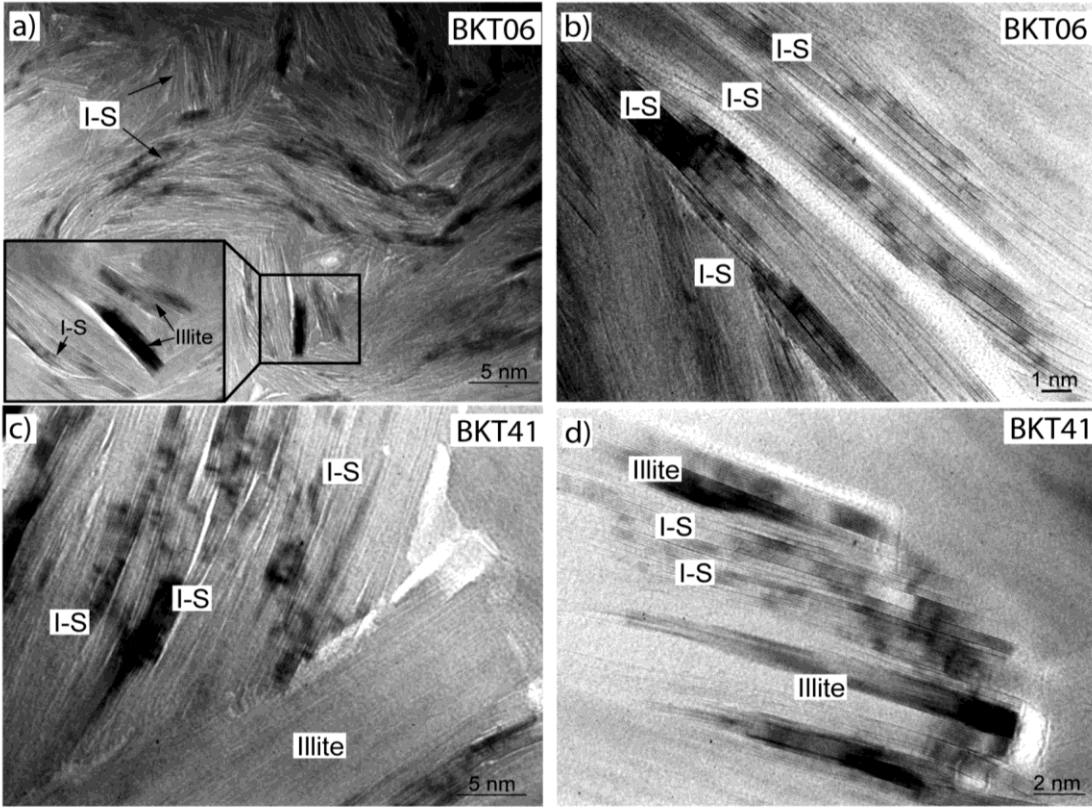
539
540 Figure 6. Lattice fringe images of samples Bukowina Tatrzańska-06 and Bukowina Tatrzańska-41 at varying
541 magnifications. A) Thin illite packets growing within illite-smectite (I-S) layers, illite is not continuous with I-S. Layer
542 terminations can be seen in the inset figure, where the arrow pointing to I-S lines on a layer termination B) I-S packets
543 are not continuous and packets are oriented at large angles to each other, C) I-S packets terminate against a thick illite
544 packet (detrital in origin), white areas separating I-S packets are probably indicative of smectite collapse and here may
545 be viewed as porosity at the angstrom scale, D) illite growing within I-S layers, illite packets generally more coherent
546 than I-S.
547
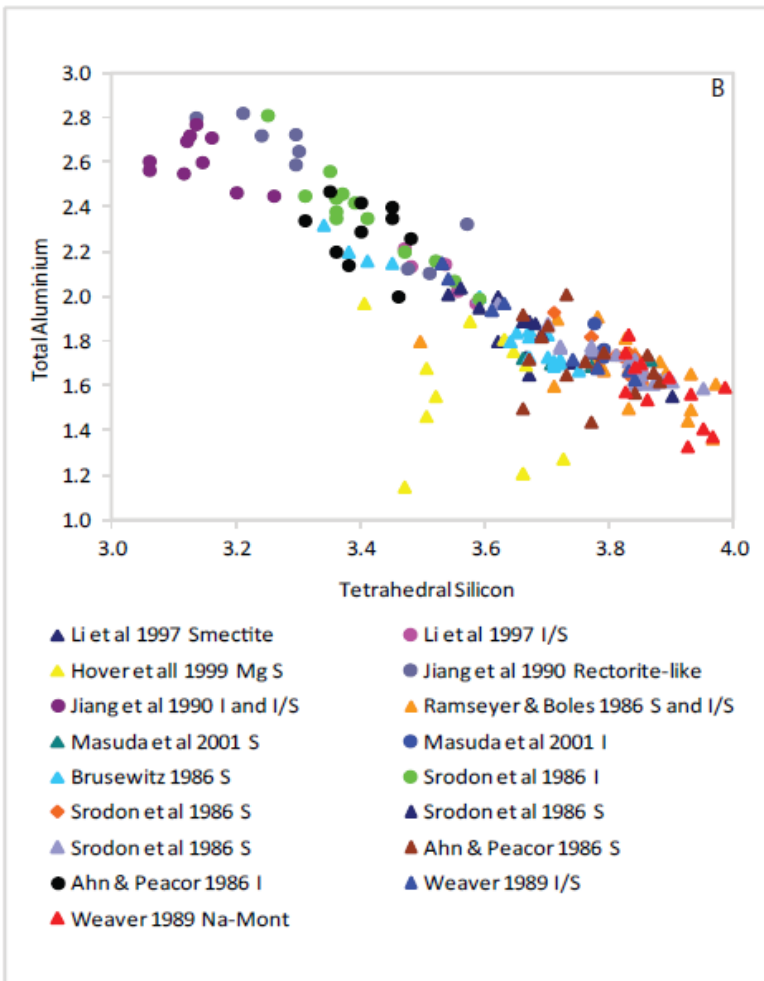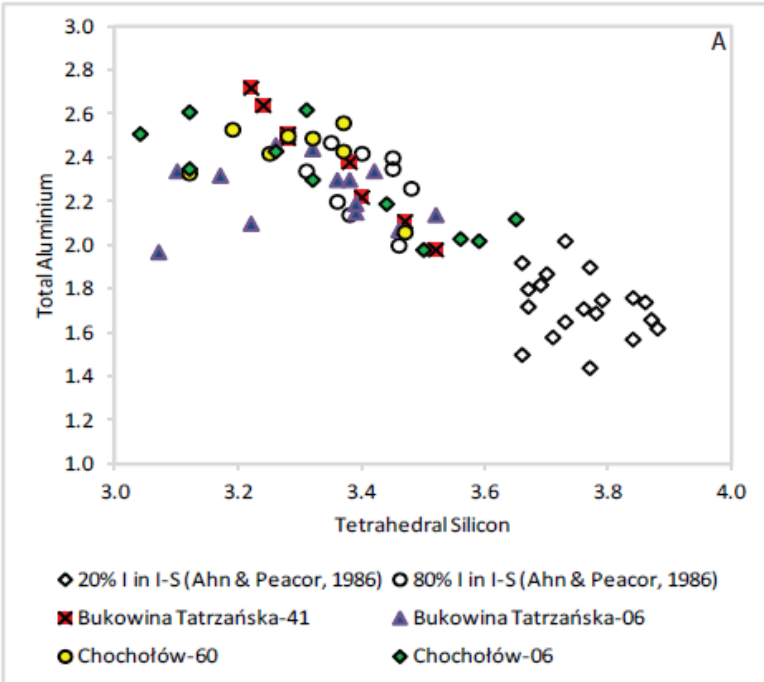
549   Figure 7. (A) Tetrahedral Si^{4+} versus total Al^{3+} for Chochołów-06, Chochołów-60, Bukowina Tatrzańska-06 and
550   Bukowina Tatrzańska-41 from TEM-EDS, data from Ahn and Peacor (1986a) are also shown. (B) Tetrahedral Si
551   versus total Al from the noted literature sources. Data are from a variety of techniques; Atomic absorption
552   Spectroscopy, DC Plasma-Emission Spectroscopy, Ignited weights, X-ray fluorescence and not TEM-EDS alone. The
553   division of the data into illite (I), illite-smectite (I/S), and smectite (S) is based on the individual author's descriptions.
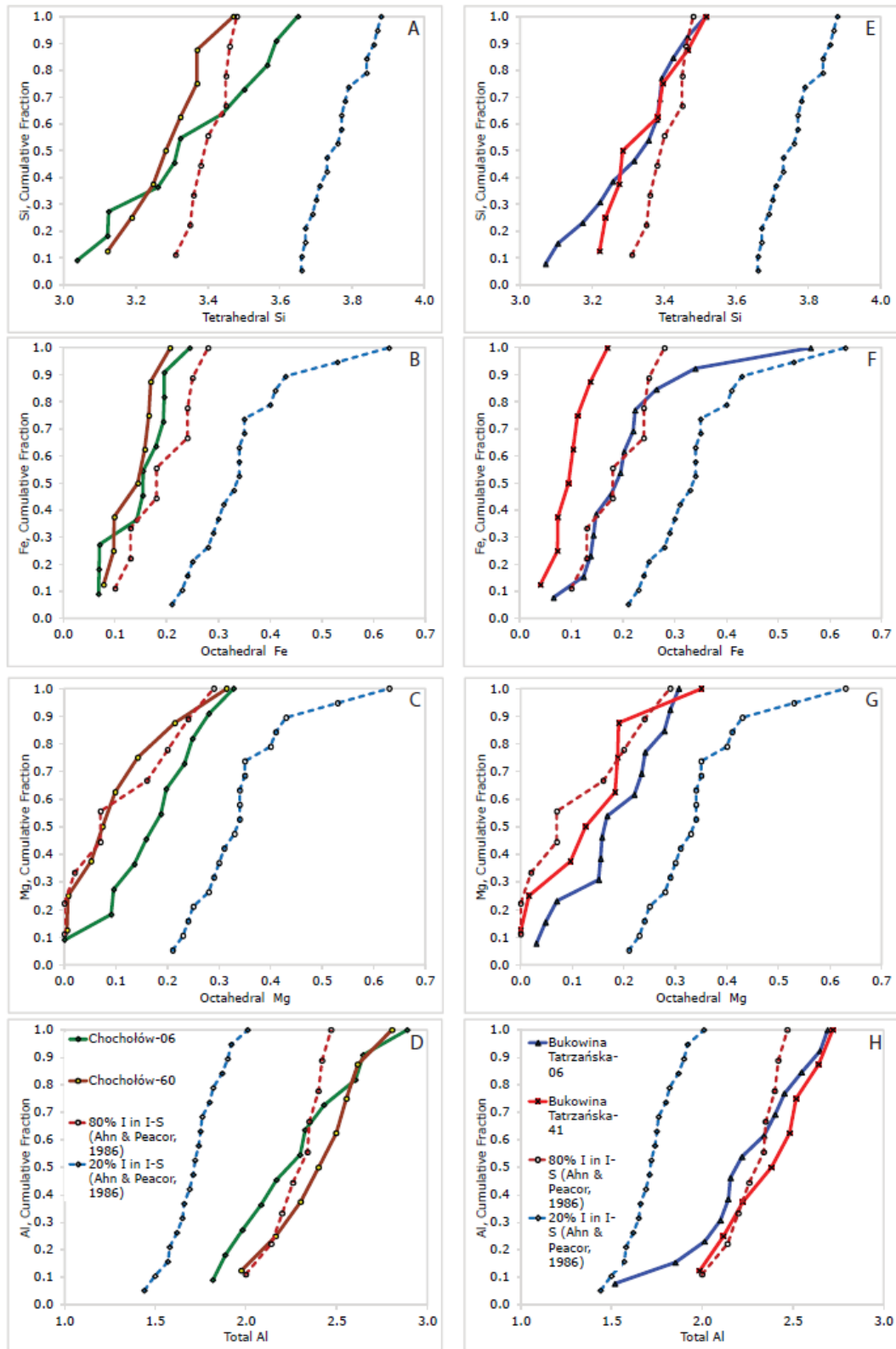
Figure 8. Kolmogorov-Smirnov distributions of (a,e) tetrahedral Si, (b,f) octahedral Fe, (c,g) octahedral Mg and (d,h) Total Al for comparisons of Chochołów-6 with Chochołów-60 and Bukowina Tatrzańska-06 with Bukowina Tatrzańska-41. Data from Ahn and Peacor (1986a) for the Texas Gulf Coast are also shown to show the separation of the data and, therefore, their difference.
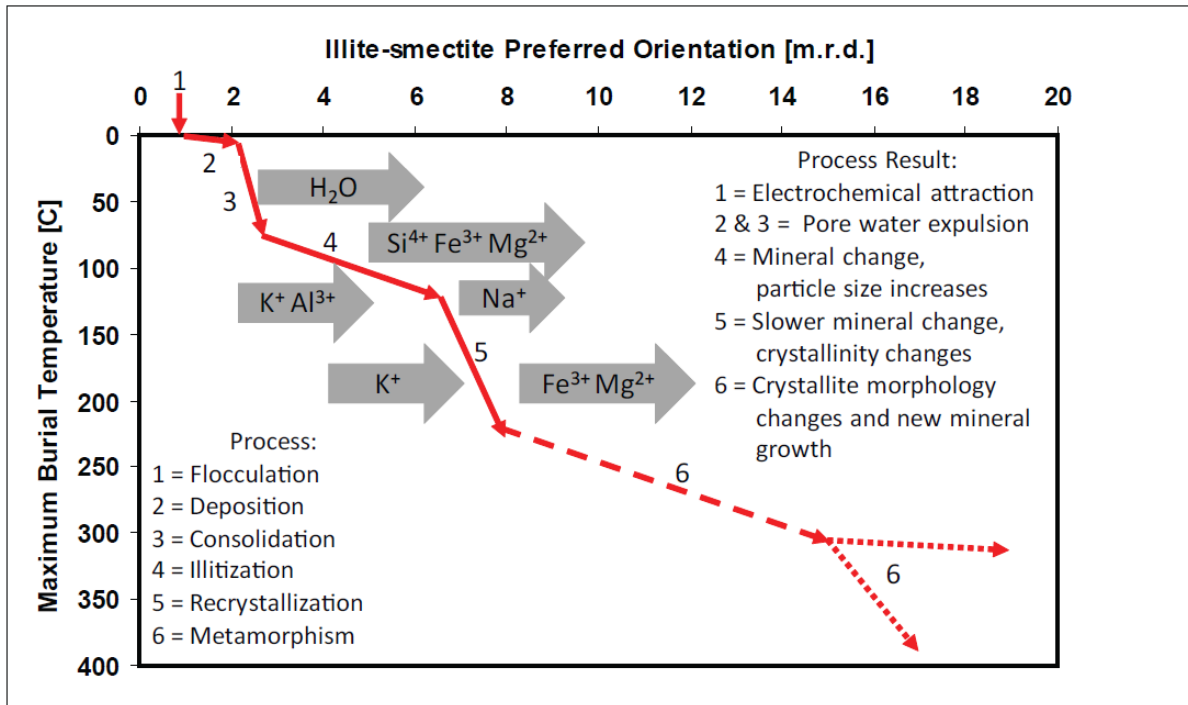
Figure 9. The development of illite-smectite preferred orientation is a stepwise process (Modified from Haines et al. 2009). Mechanical processes give way to chemical processes that see initial significant changes in mineralogy and associated preferred orientation. As reaction products are consumed diagenesis slows but potassium is still taken up by clay minerals that concomitantly release iron and aluminum (mica formation). A second significant stage of preferred orientation development occurs into metamorphism but is not well defined.

8. References

Ahn, J.H. and Peacor, D.R., 1986. Transmission and analytical electron microscopy of the smectite to illite transition. Clays and Clay Minerals, 34: 165-179.

Anczkiewicz, A., 2006. Verification by AFT technique of the maxium palaeotemperatures evaluted from illite-smectite for the Tatra Mts., the Podhale Basin and the neighbouring area of the Outer Carpathians. PhD thesis, Institute of Geological Sciences PAN, Krakow (in Polish).

Aplin, A.C., Matenaar, I.F., McCarty, D.K. and van der Pluijm, B.A., 2006. Influence of mechanical compaction and clay mineral diagenesis on the microfabric and pore-scale properties of deep-water Gulf of Mexico mudstones. Clays and Clay Minerals, 54(4): 500-514.

Bell, T.E., 1986. Microstructure in mixed-layer illite/smectite and its relationship to the reaction of smectite and illite. Clays and Clay Minerals, 34(2): 146-154.

Bjørlykke, K. and Høeg, K., 1997. Effects of burial diagenesis on stresses, compaction and fluid flow in sedimentary basins. Marine and Petroleum Geology, 14(3): 267-276.

Boles, J.R. and Franks, S.G., 1979. Clay diagenesis in Wilcox Sandstones of southwest Texas. Journal of Sedimentary Petrology, 49: 55-70.

Bowers, G.L., 1995. Pore Pressure Estimation From Velocity Data: Accounting for Overpressure Mechanisms Besides Undercompaction. Society of Petroleum Engineers (SPE 27488), 10(2): 89-95.

Brusewitz, A.M., 1986. Chemical and Physical-Properties of Paleozoic Potassium Bentonites from Kinnekulle, Sweden. Clays and Clay Minerals, 34(4): 442-454.

Cliff, G. and Lorimer, G.W., 1975. Quantitative-Analysis of Thin Specimens. Journal of Microscopy-Oxford, 103(MAR): 203-207.

Curtis, C.D., Lipshie, S.R., Oertel, G. and Pearson, M.J., 1980. Clay Orientation in Some Upper Carboniferous Mudrocks, Its Relationship to Quartz Content and Some Inferences About Fissility, Porosity and Compactional History. Sedimentology, 27(3): 333-339.

Day-Stirrat, R.J., Aplin, A.C., Środoń, J. and van der Pluijm, B.A., 2008a. Diagenetic reorientation of phyllosilicate minerals in Paleogene mudstones of the Podhale Basin, southern Poland. Clays and Clay Minerals, 56(1): 100-111.

Day-Stirrat, R.J., Loucks, R.G., Milliken, K.L., Hillier, S. and van der Pluijm, B.A., 2008b. Phyllosilicate orientation demonstrates early timing of compactional stabilization in calcite-cemented concretions in the Barnett Shale (Late Mississippian), Fort Worth Basin, Texas (U.S.A). Sedimentary Geology, 208(1-2): 27-35.

Day-Stirrat, R.J. et al., 2011. Preferred orientation of phyllosilicates: Effects of composition and stress on resedimented mudstone microfabrics. Journal of Structural Geology, 33: 1347-1358.

Djéran-Maigre, I., Tessier, D., Grunberger, D., Velde, B. and Vasseur, G., 1998. Evolution of microstructures and of macroscopic properties of some clays during experimental compaction. Marine and Petroleum Geology, 15(2): 109-128.

Goulty, N.R. and Sargent, C., 2016. Compaction of diagenetically altered mudstones – Part 2: Implications for pore pressure estimation. Marine and Petroleum Geology, 77: 806-818.

Goulty, N.R., Sargent, C., Andras, P. and Aplin, A.C., 2016. Compaction of diagenetically altered mudstones – Part 1: Mechanical and chemical contributions. Marine and Petroleum Geology, 77: 703-713.

Haines, S.H., van der Pluijm, B.A., Ikari, M.J., Saffer, D.M. and Marone, C., 2009. Clay fabric intensity in natural and artificial fault gouges: Implications for brittle fault zone processes

635　　　　and sedimentary basin clay fabric evolution. Journal of Geophysical Research-Solid
636　　　　Earth, 114.
637　Ho, N.C., Peacor, D.R. and van der Pluijm, B.A., 1995. Reorientation Mechanisms of
638　　　　Phyllosilicates in the Mudstone-to-Slate Transition at Lehigh Gap, Pennsylvania. Journal
639　　　　of Structural Geology, 17(3): 345-356.
640　Ho, N.C., Peacor, D.R. and van der Pluijm, B.A., 1999. Preferred Orientation of Phyllosilicates
641　　　　in Gulf Coast Mudstones and Relation to the Smectite-Illite Transition. Clays and Clay
642　　　　Minerals, 47(4): 495-504.
643　Hover, V.C., Walter, L.M., Peacor, D.R. and Martini, A.M., 1999. Mg-Smectite Authigenesis in
644　　　　a Marine Evaporite Environment, Salina Ometepec, Baja California. Clays and Clay
645　　　　Minerals, 47(3): 252-268.
646　Hower, J., Eslinger, E.V., Hower, M.E. and Perry, E.A., 1976. Mechanism of Burial
647　　　　Metamorphism of Argillaceous Sediment 1. Mineralogical and Chemical Evidence.
648　　　　Geological Society of America Bulletin, 87(5): 725-737.
649　Inoue, A., Kohyama, N., Kitagawa, R. and Watanabe, T., 1987a. Chemical and morphological
650　　　　evidence for the conversion of smectite to illite. Clays and Clay Minerals, 42: 276-287.
651　Inoue, A., Velde, B., Meunier, A. and Touchard, G., 1987b. Mechanism of illite formation
652　　　　during smectite-to-illite conversion in a hydrothermal system. American Mineralogist,
653　　　　73: 1325-34.
654　Jacob, G., Kisch, H.J. and van der Pluijm, B.A., 2000. The relationship of phyllosilicate
655　　　　orientation, X-ray diffraction intensity ratios, and c/b fissility ratios in metasedimentary
656　　　　rocks of the Helvetic zone of the Swiss Alps and the Caledonides of Jamtland, central
657　　　　western Sweden. Journal of Structural Geology, 22(2): 245-258.
658　Jiang, W.T., Peacor, D.R., Merriman, R.J. and Roberts, B., 1990. Transmission and Analytical
659　　　　Electron-Microscopic Study of Mixed-Layer Illite Smectite Formed as an Apparent
660　　　　Replacement Product of Diagenetic Illite. Clays and Clay Minerals, 38(5): 449-468.
661　Jiang, W.T., Peacor, D.R. and Buseck, P.R., 1994. Chlorite geothermometry?-contamination and
662　　　　apparent octahedral vacancies. Clays and Clay Minerals, 42(5): 593-605.
663　Kim, J., Dong, H.L., Seabaugh, J., Newell, S.W. and Eberl, D.D., 2004. Role of microbes in the
664　　　　smectite-to-illite reaction. Science, 303(5659): 830-832.
665　Kim, J.W., Peacor, D.R., Tessier, D. and Elsass, F., 1995. A Technique for Maintaining Texture
666　　　　and Permanent Expansion of Smectite Interlayers for Tem Observations. Clays and Clay
667　　　　Minerals, 43(1): 51-57.
668　Klimentidis, R.E. and Mackinnon, I.D.R., 1986. High-Resolution Imaging of Ordered Mixed-
669　　　　Layer Clays. Clays and Clay Minerals, 34(2): 155-164.
670　Lahann, R., 2002. Impact of smectite diagenesis on compaction modeling and compaction
671　　　　equilibrium. In: A.R. Huffman and G.L. Bowers (Editors), American Association of
672　　　　Petroleum Geologists Memoir 76: Pressure regimes in sedimentary basins and their
673　　　　prediction. American Association of Petroleum Geologists, Tulsa, Oklahoma, pp. 61-72.
674　Lahann, R.W. and Swarbrick, R.E., 2011. Overpressure generation by load transfer following
675　　　　shale framework weakening due to smectite diagenesis. Geofluids, 11(4): 362-375.
676　Land, L.S., Mack, L.E., Milliken, K.L. and Lynch, F.L., 1997. Burial diagenesis of argillaceous
677　　　　sediment, south Texas Gulf of Mexico sedimentary basin: A reexamination. Geological
678　　　　Society of America Bulletin, 109(1): 2-15.
679　Land, L.S. and Milliken, K.L., 2000. Regional loss of SiO2, and gain of K2O during burial
680　　　　diagenesis of Gulf Coast mudrocks, USA. In: R.H. Worden and S. Morad (Editors),

681   Quartz Cementation in Sandstones. International Association of Sedimentologists, pp.
682   183-197.
683 Li, G.J., Peacor, D.R. and Coombs, D.S., 1997. Transformation of smectite to illite in bentonite
684   and associated sediments from Kaka Point, New Zealand: Contrast in rate and
685   mechanism. Clays and Clay Minerals, 45(1): 54-67.
686 Marynowski, L. et al., 2006. Origin of organic matter from tectonic zones in the Western Tatra
687   Mountains Crystalline Basement, Poland: An example of bitumen - source rock
688   correlation. Marine and Petroleum Geology, 23(2): 261-279.
689 Masuda, H., Peacor, D.R. and Dong, H., 2001. Transmission electron microscopy study of
690   conversion of smectite to illite in mudstones of Nankai Trough: contrast with coeval
691   bentonites. Clays and Clay Minerals, 49(2): 109-118.
692 Merriman, R.J., Roberts, B., Peacor, D.R. and Hirons, S.R., 1995. Strain-Related Differences in
693   the Crystal-Growth of White Mica and Chlorite - a Tem and Xrd Study of the
694   Development of Metapelitic Microfabrics in the Southern Uplands Thrust Terrane,
695   Scotland. Journal of Metamorphic Geology, 13(5): 559-576.
696 Merriman, R.J. and Peacor, D.R., 1998. Very low-grade metapelites: mineralogy, microfabrics
697   and measuring reaction progress. In: M. Frey and D. Robinson (Editors), Low-Grade
698   Metamorphism. Blackwell Science.
699 Merriman, R.J., 2002. Contrasting clay mineral assemblages in British Lower Palaeozoic slate
700   belts: the influence of geotectonic setting. Clay Minerals, 37(2): 207-219.
701 Moore, D.M. and Reynolds, R.C.J., 1997. X-ray diffraction and the identification and analysis of
702   clay minerals. Oxford University Press, Oxford, New York.
703 Nadeau, P.H., Peacor, D.R., Yan, J. and Hillier, S., 2002. I-S precipitation in pore space as the
704   cause of geopressuring in Mesozoic mudstones, Egersund Basin, Norwegian Continental
705   Shelf. American Mineralogist, 87(11-12): 1580-1589.
706 Oertel, G. and Curtis, C.D., 1972. Clay-Ironstone Concretion Preserving Fabrics Due to
707   Progressive Compaction. Geological Society of America Bulletin, 83(9): 2597-2605.
708 Olszewska, B.W. and Wieczorek, J., 1998. The Palaeogene of the Podhale Basin (Polish Inner
709   Carpathians)-micropaleontological perspectives. Przeglad Geologiczny, 46(8/2): 721-
710   728.
711 Peacor, D.R., 1992. Analytical Electron-Microscopy - X-Ray-Analysis. Reviews in Mineralogy,
712   27: 113-140.
713 Perry, E. and Hower, J., 1970. Burial diagenesis in Gulf Coast pelitic sediments. Clays and Clay
714   Minerals, 18: 165-177.
715 Poprawa, P. and Marynowski, L., 2005. Thermal history of the Podhale Trough (northern part of
716   the Central Carpathian Paleogene Basin) - preliminary results from 1-D maturity
717   modeling. Mineralogical Society of Poland - Special Papers, 25: 352-355.
718 Ramseyer, K. and Boles, J.R., 1986. Mixed-Layer Illite Smectite Minerals in Tertiary Sandstones
719   and Shales, San-Joaquin Basin, California. Clays and Clay Minerals, 34(2): 115-124.
720 Rieke, H.H. and Chilingarian, G.V., 1974. Compaction of argillaceous sediments. Compaction of
721   argillaceous sediments. Developments in Sedimentology 16. Elsevier.
722 Sorby, H.C., 1853. On the origin of slaty cleavage. Edinburgh New Philosophical Journal, 10:
723   136.
724 Środoń, J., Morgan, D.J., Eslinger, E.V., Eberl, D.D. and Karlinger, M.R., 1986. Chemistry of
725   Illite Smectite and End-Member Illite. Clays and Clay Minerals, 34(4): 368-378.

726 Środoń, J., Clauer, N., Banas, M. and Wojtowicz, A., 2006a. K-Ar evidence for a Mesozoic
727   thermal event superimposed on burial diagenesis of the Upper Silesia Coal Basin. Clay
728   Minerals, 41(2): 669-690.
729 Środoń, J. et al., 2006b. Diagenetic history of the Podhale-Orava Basin and the underlying Tatra
730   sedimentary structural units (Western Carpathians): evidence from XRD and K-Ar of
731   illite-smectite. Clay Minerals, 41: 751-774.
732 Środoń, J., 2009. Quantification of illite and smectite and their layer charges in sandstones
733 and shales from shallow burial depth. Clay Minerals, 44: 421-434.
734 Stuart, A., Ord, J.K. and Arnold , S., 1999. Kendall's Advanced Theory of Statistics, Volume 2A,
735   London : Arnold ; New York : Oxford University Press.
736 Tari, G., Baldi, T. and Baldibeke, M., 1993. Paleogene Retroarc Flexural Basin beneath the
737   Neogene Pannonian Basin - a Geodynamic Model. Tectonophysics, 226(1-4): 433-455.
738 Taylor, T.R. et al., 2010. Sandstone diagenesis and reservoir quality prediction: Models, myths,
739   and reality. AAPG Bulletin, 94(8): 1093-1132.
740 van de Kamp, P.C., 2008. Smectite-Illite-Muscovite transformation, Quartz Dissolution, and
741   Silica Release in Shales. Clays and Clay Minerals, 56(1): 66-81.
742 van der Pluijm, B.A., Lee, J.H. and Peacor, D.R., 1988. Analytical Electron-Microscopy and the
743   Problem of Potassium Diffusion. Clays and Clay Minerals, 36(6): 498-504.
744 Voltolini, M., Wenk, H.R., Mondol, N.H., Bjorlykke, K. and Jahren, J., 2009. Anisotropy of
745   experimentally compressed kaolinite-illite-quartz mixtures. Geophysics, 74(1): D13-D23.
746 Warren, E.A. and Ransom, B., 1992. The Influence of Analytical Error Upon the Interpretation
747   of Chemical Variations in Clay-Minerals. Clay Minerals, 27(2): 193-209.
748 Weaver, C.E., 1989. Clays, muds, and shales. Developments in Sedimentology 44. Elsevier,
749   Amsterdam, New York.
750 Westwalewicz-Magilska, E., 1986. Nowe spojrzenie na geneze osadów fliszu podhalanskiego.
751   Przeglad Geologiczny, 12: 690-698 (in Polish).
752 Yang, Y. and Aplin, A.C., 2004. Definition and practical application of mudstone porosity–
753   effective stress relationships. Petroleum Geoscience, 10(2): 153-162.
754 Yang, Y.L. and Aplin, A.C., 1997. A method for the disaggregation of mudstones.
755   Sedimentology, 44(3): 559-562.
756
757
758